Ion-Transfer Electrochemistry at Arrays of Nanointerfaces between Immiscible Electrolyte Solutions Confined within Silicon Nitride Nanopore Membranes

ARTICLE *in* ANALYTICAL CHEMISTRY · JULY 2010

Impact Factor: 5.64 · DOI: 10.1021/ac1008282 · Source: PubMed

6 AUTHORS, INCLUDING:

Micheál D. Scanlon
University College Cork
45 PUBLICATIONS **663** CITATIONS
SEE PROFILE

Alan M Blake
University College Cork
22 PUBLICATIONS **610** CITATIONS
SEE PROFILE

Daniela Iacopino
Tyndall National Institute
55 PUBLICATIONS **803** CITATIONS
SEE PROFILE

Damien W M Arrigan
Curtin University
158 PUBLICATIONS **3,159** CITATIONS
SEE PROFILE

Anal. Chem. **2010,** *82,* 6115–6123

Ion-Transfer Electrochemistry at Arrays of Nanointerfaces between Immiscible Electrolyte Solutions Confined within Silicon Nitride Nanopore Membranes

Micheál D. Scanlon, Jörg Strutwolf, Alan Blake, Daniela Iacopino, Aidan J. Quinn, and Damien W. M. Arrigan*,†

Tyndall National Institute, Lee Maltings, University College Cork, Cork, Ireland

Ion transfer across interfaces between immiscible liquids provides a means for the nonredox electrochemical detection of ions. Miniaturization of such interfaces brings the benefits of enhanced mass transport. Here, the electrochemical behavior of geometrically regular arrays of nanoscale interfaces between two immiscible electrolyte solutions (nanoITIES arrays) is presented. These were prepared by supporting the two electrolyte phases within silicon nitride membranes containing engineered arrays of nanopores. The nanoITIES arrays were characterized by cyclic voltammetry of the interfacial transfer of tetraethylammonium cation (TEA^+) between the aqueous phase and the gelled organic phase. Effects of pore radius, pore center-to-center separation, and number of pores in the array were examined. The ion transfer produced apparent steady-state voltammetry on the forward and reverse sweeps at all experimentally accessible scan rates and at all nanopore array designs. However, background-subtraction of the voltammograms revealed the evolution of a peak-shaped response on the reverse sweep with increasing scan rate, indicative of pores filled with the organic phase to a certain extent. The steady-state voltammetric behavior at the nanoITIES arrays on the forward sweep for arrays with significant diffusion zone overlap between adjacent nanoITIES is indicative of the dominance of radial diffusion to interfaces at the edge of the arrays over linear diffusion to interfaces within the arrays. This implies that nanoITIES arrays, which occupy an overall area of micrometer dimensions, behave like a single μITIES of corresponding area to the nanoITIES array.

The development of arrays of nanoscale interfaces between two immiscible electrolyte solutions (nanoITIES) will offer benefits at the liquid−liquid interface similar to those experienced at the solid−liquid interface on introduction of solid nanoelectrode arrays.[1−3] The motivation for such miniaturization is 2-fold: the enhanced diffusional mass transport that occurs to nanosized array elements, offering benefit for improvement in applications to analytical detection, and the possibility of creating arrays of nanointerfaces that approach biological nanopore dimensions and, thus, enable insights into aspects of the function of such pores. Single nanoITIES have enabled significantly enhanced mass transport[4] and voltammetric measurements in low polarity media or even in media with no supporting electrolytes.[5−7] Furthermore, by supporting the nanoITIES within nanoporous solid-state membranes, additional benefits accrue, including control over nanopore size, array geometry, and mechanical stability at the interface.

To date, two categories of nanoITIES have been reported: those supported at the tip of a nanopipette[4−14] or a double-barreled nanopipette,[6,15,16] producing single or double nanointerfaces, and those created by placing nanoporous materials at the ITIES. These nanoporous materials contain geometrically irregular pore arrays with extremely high pore densities (up to ca. 10^9 pores per cm^2), such as "track etched" polyester[17,18] and γ-alumina ultrafiltration

* Corresponding author. E-mail: d.arrigan@curtin.edu.au. Tel: +61-8-9266-9735. Fax: +61-8-9266-4699.

† Current address: Nanochemistry Research Institute, Department of Chemistry, Curtin University of Technology, GPO Box U1987, Perth, WA 6845, Australia.

(1) Arrigan, D. W. M. *Analyst* **2004**, *129*, 1157–1165.
(2) Compton, R. G.; Wildgoose, G. G.; Rees, N. V.; Streeter, I.; Baron, R. *Chem. Phys. Lett.* **2008**, *459*, 1–17.
(3) Murray, R. W. *Chem. Rev.* **2008**, *108*, 2688–2720.
(4) Shao, Y.; Mirkin, M. V. *J. Am. Chem. Soc.* **1997**, *119*, 8103–8104.
(5) Sun, P.; Laforge, F. O.; Mirkin, M. V. *J. Am. Chem. Soc.* **2005**, *127*, 8596–8597.
(6) Laforge, F. O.; Sun, P.; Mirkin, M. V. *J. Am. Chem. Soc.* **2006**, *128*, 15019–15025.
(7) Sun, P.; Laforge, F. O.; Mirkin, M. V. *J. Am. Chem. Soc.* **2007**, *129*, 12410–12411.
(8) Sun, P.; Zhang, Z.; Gao, Z.; Shao, Y. *Angew. Chem., Int. Ed.* **2002**, *41*, 3445–3448.
(9) Yuan, Y.; Shao, Y. *J. Phys. Chem. B* **2002**, *106*, 7809–7814.
(10) Zhan, D.; Yuan, Y.; Xiao, Y.; Wu, B.; Shao, Y. *Electrochim. Acta* **2002**, *47*, 4477–4483.
(11) Cai, C.; Tong, Y.; Mirkin, M. V. *J. Phys. Chem. B* **2004**, *108*, 17872–17878.
(12) Li, F.; Chen, Y.; Sun, P.; Zhang, M.; Gao, Z.; Zhan, D.; Shao, Y. *J. Phys. Chem. B* **2004**, *108*, 3295–3302.
(13) Cai, C.; Mirkin, M. V. *J. Am. Chem. Soc.* **2006**, *128*, 171–179.
(14) Jing, P.; Zhang, M.; Hu, H.; Xu, X.; Liang, Z.; Li, B.; Shen, L.; Xie, S.; Pereira, C. M.; Shao, Y. *Angew. Chem., Int. Ed.* **2006**, *45*, 6861–6864.
(15) Shao, Y.; Liu, B.; Mirkin, M. V. *J. Am. Chem. Soc.* **1998**, *120*, 12700–12701.
(16) Hu, H.; Xie, S.; Meng, X.; Jing, P.; Zhang, M.; Shen, L.; Zhu, Z.; Li, M.; Zhuang, Q.; Shao, Y. *Anal. Chem.* **2006**, *78*, 7034–7039.
(17) Dryfe, R. A. W.; Kralj, B. *Electrochem. Commun.* **1999**, *1*, 128–130.
(18) Kralj, B.; Dryfe, R. A. W. *Phys. Chem. Chem. Phys.* **2001**, *3*, 5274–5282.

10.1021/ac1008282
Published on Web 06/16/2010

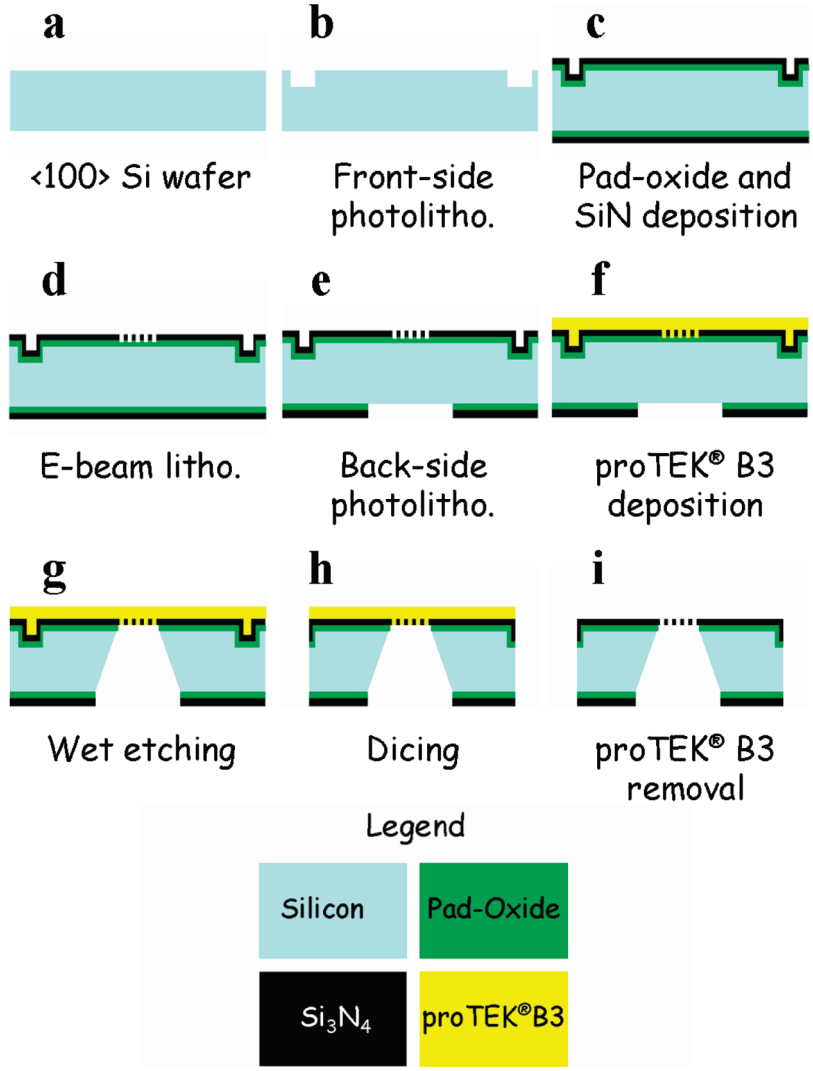

Figure 1. Fabrication process flowchart for the preparation of nanopore arrays in Si_3N_4 membranes. Note: this flowchart is not to scale. The bulk silicon layer is 525 μm thick, the pad−oxide layer is 35 nm thick; the proTEKB3 layer is 8 μm thick, and, finally, the patterned Si_3N_4 layer is 100 nm thick.

membranes.[19] In the past decade, a series of solid-state nanopore membranes have been fabricated in a variety of materials to act as sensors for DNA and other biological molecules such as peptides and proteins,[20−22] although such membranes have not been utilized for nanostructuring of the ITIES.

In this work, arrays of geometrically regular nanoITIES are presented. These were created by supporting the two liquid electroyte phases on either side of solid-state nanopore membranes prepared in 100 nm thick silicon nitride. Thus, arrays of nanoITIES, or nanoscale liquid−liquid interfaces, result. The development of nanoITIES arrays opens up opportunities for enhanced bioanalytical detection based on biomolecular interactions at the ITIES.[23−27] The geometric parameters of the nanoporous membranes were evaluated by scanning electron microscopy (SEM). The electrochemical transfer of the tetraethylammonium cation (TEA^+) across the water/1,6-dichlorohexane interface was chosen as a model system to investigate the voltammetric responses of the nanopore array designs in terms of pore radius (r_a), pore center-to-center separation (r_c), and total number of pores in the array (N_p).

EXPERIMENTAL SECTION

Membrane Fabrication. As summarized in Figure 1, the nanopore array membranes studied were prepared by standard etching, deposition, and patterning methods. Silicon nitride (Si_3N_4) was chosen as the membrane material for its ability to survive the fabrication process itself and to survive repeated immersions in liquids while being only tens of nanometers in thickness. The Si_3N_4 membrane was supported by a silicon (Si) wafer frame, which was 525 μm thick. The nanopore arrays were etched into this thin Si_3N_4 membrane. Oxide and nitride

(19) Platt, M.; Dryfe, R. A. W.; Roberts, E. P. L. *Langmuir* **2003**, *19*, 8019–8025.
(20) Dekker, C. *Nat. Nano* **2007**, *2*, 209–215.
(21) Healy, K.; Schiedt, B.; Morrison, A. P. *Nanomedicine* **2007**, *2*, 875–897.
(22) Gyurcsányi, R. E. *Trends Anal. Chem.* **2008**, *27*, 627–639.
(23) Arrigan, D. W. M. *Anal. Lett.* **2008**, *41*, 3233–3252.
(24) Herzog, G.; Kam, V.; Arrigan, D. W. M. *Electrochim. Acta* **2008**, *53*, 7204–7209.
(25) Kivlehan, F.; Lanyon, Y. H.; Arrigan, D. W. M. *Langmuir* **2008**, *24*, 9876–9882.
(26) Collins, C. J.; Arrigan, D. W. M. *Anal. Chem.* **2009**, *81*, 2344–2349.
(27) Strutwolf, J.; Scanlon, M. D.; Arrigan, D. W. M. *Analyst* **2009**, *134*, 148–158.

layers were deposited onto the ⟨100⟩ silicon substrate thermally and via low pressure chemical vapor deposition (LPCVD), respectively. The nanopore array designs were patterned into an electron-beam resist on top of the front-side Si_3N_4 layer by e-beam lithography. Subsequently, the nanopores were etched into the Si_3N_4 layer using a magnetic zero-resonant induction (M0RI) etch, a form of inductively coupled plasma etch, using fluorocarbon gas chemistry (CHF_3/CH_2F_2/argon). The backside nitride layer was patterned by photolithography and etched with a PERIE nitride-on-oxide etch (consisting of a SF_6/HBr/O_2 plasma), which stopped on the underlying pad−oxide layer. This underlying oxide layer was then removed using a 10:1 HF wet etch, and the bulk silicon was subsequently removed from the back of the wafer by KOH wet-etching. Protection of the 100 nm thick Si_3N_4 membrane during the final fabrication and wafer dicing steps was achieved using the proTEK B3 polymer film (Brewer Science, Montana). This was applied by spin-coating prior to the KOH wet-etch step and removed after dicing by wet-etching in a solvent solution (proTEK Remover 100). We are not aware of previous fabrication of nanopore membranes using such a protective layer in final chip preparation. The final Si_3N_4 membrane was a 500 μm × 500 μm area within each diced chip, supported by a Si surround. This sequence of fabrication and dicing steps resulted in a low number of broken membranes, ca. 6%.

A single 4 in. ⟨100⟩ silicon wafer provided up to 200 5 mm ×5 mm chips each containing a 5 μm × 5 μm nanopore array patterned on the 500 μm × 500 μm membrane area. The chips were cleaned in O_2 plasma (March Plasmod) prior to experimental characterization. All processing was carried out within the Central Fabrication Facility at Tyndall National Institute. The membrane thickness, 100 nm for all array designs, was confirmed by analysis using a Nanospec 3000 system (Nanometrics Incorporated, California).

Characterization. Contact angle measurements were made with an OCA contact angle system (Dataphysics Instruments GmbH, Germany). The drop volume dispensed on the surface was 1 μL. The contact angle between the drop and the substrate was measured immediately after the contact was made. High resolution SEM images of the nanopore arrays were obtained using a cold-cathode field-emission scanning electron microscope (6700F SEM, JEOL U.K. Ltd.) operated at beam voltages between 3 and 7.5 kV. Beam voltages were adjusted to minimize charging effects from the insulating silicon nitride substrate. These charging effects ultimately limited the imaging resolution.

Reagents. All reagents used in the electrochemical studies were purchased from Sigma-Aldrich Ireland Ltd. and used without further purification, with the exception of 1,6-dichlorohexane (1,6-DCH) which was purified as described elsewhere.[28] The aqueous phase electrolyte of 10 mM LiCl was prepared in ultrapure water (resistivity: 18 MΩ cm) from an Elgastat maxima-HPLC (Elga, UK). The model analyte species studied was the tetraethylammonium cation (TEA^+), used as its chloride salt in a 10 mM LiCl aqueous phase. The organic electrolyte salt was prepared by metathesis of bis(triphenylphosphoranylidene)ammonium chloride (BTPPA)(Cl) and potassium tetrakis(4-chlorophenyl)borate (K)(TPBCl) to obtain (BTPPA)(TPBCl), following the published experimental procedure.[29] The organic phase was prepared as a gel[30] and was composed of the organic solvent (1,6-DCH), the organic electrolyte (10 mM (BTPPA)(TPBCl)), and low molecular weight poly(vinylchloride) (PVC, from Fluka Chemika). The organic reference solution consisted of 10 mM (BTPPA)(Cl) dissolved in 10 mM LiCl(aq).

NanoITIES Array Electrochemistry. Voltammetry experiments at nanoscopic liquid−liquid interface arrays were carried out using a CH instruments 620B potentiostat (CH Instruments, Texas). The electrochemical cell used to support the three-electrode configuration (Figure S-1, Supporting Information) was the one that was used previously when characterizing ion transfer[27,31] or detecting biological molecules[26,30] at a gelified μITIES array, except that the 4 mm × 4 mm microporous chips were replaced with the 5 mm × 5 mm nanoporous chips. Briefly, the nanoporous Si_3N_4 membrane was sealed onto the lower orifice of a borosilicate glass cylinder (6 mm external diameter, 3 mm inner diameter) using silicone rubber (RS Components, stock number 555-588). This glass cylinder contained the organic phase (20−30 μL), present as an organogel, with the organic phase reference solution (a further 20−30 μL) placed on top of the organogel. The aqueous phase was contained in a 10 mL beaker. The setup consisted of one Pt mesh counter electrode (in the aqueous phase) and two Ag/AgCl reference electrodes (one in each phase). When working with low electrical currents, three-electrode configurations are possible.[32−34] Just such a scenario arose here, and the Ag/AgCl electrode in the organic phase carried out the duties of both a counter and a reference electrode. The electrochemical cell was housed in a Faraday cage for the duration of the experiments.

Once the cell was set up, a sequence of "blank" cyclic voltammograms (CVs; i.e., no TEA^+ present in the aqueous phase) was run, three in total, at intervals of 180 s. The starting potential, $\Delta_o^w\varphi_{st}$, for each of these CVs was set at 0.35 V, and the switching potential, $\Delta_o^w\varphi_{sw}$, was set at 1.00 V. A quiet time of 5 s was set prior to each CV, and the scan rates applied varied between 5 and 100 mV s^{-1}. Subsequently, an aliquot of TEA^+ stock solution was injected into the aqueous phase using a calibrated micropipet to produce a TEA^+ concentration of 150 μM and a sequence of three CVs was acquired, as for the "blank" CVs. CVs of 150 μM TEA^+ were obtained by background subtraction of the "blank" CV data using the CH Instruments software.

RESULTS AND DISCUSSION

Fabrication and Characterization of Solid-State Nanopore Array Membranes. The nanopore membranes were fabricated in silicon nitride (Si_3N_4) using combinations of photo- and electron-beam lithography, etching, and deposition. The key steps in the fabrication flow are outlined in Figure 1. In summary, the fabrication involved deposition of Si_3N_4 onto bulk

(28) Katano, H.; Tatsumi, H.; Senda, M. *Talanta* **2004**, *63*, 185–193.

(29) Lee, H. J.; Beattie, P. D.; Seddon, B. J.; Osborne, M. D.; Girault, H. H. *J. Electroanal. Chem.* **1997**, *440*, 73–82.

(30) Scanlon, M. D.; Herzog, G.; Arrigan, D. W. M. *Anal. Chem.* **2008**, *80*, 5743–5749.

(31) Strutwolf, J.; Scanlon, M. D.; Arrigan, D. W. M. *J. Electroanal. Chem.* **2010**, *641*, 7–13.

(32) Marecek, V.; Samec, Z. *Anal. Lett.* **1981**, *14*, 1241–1253.

(33) Campbell, J. A.; Girault, H. H. *J. Electroanal. Chem.* **1989**, *266*, 465–469.

(34) Zazpe, R.; Hibert, C.; O'Brien, J.; Lanyon, Y. H.; Arrigan, D. W. M. *Lab Chip* **2007**, *7*, 1732–1737.

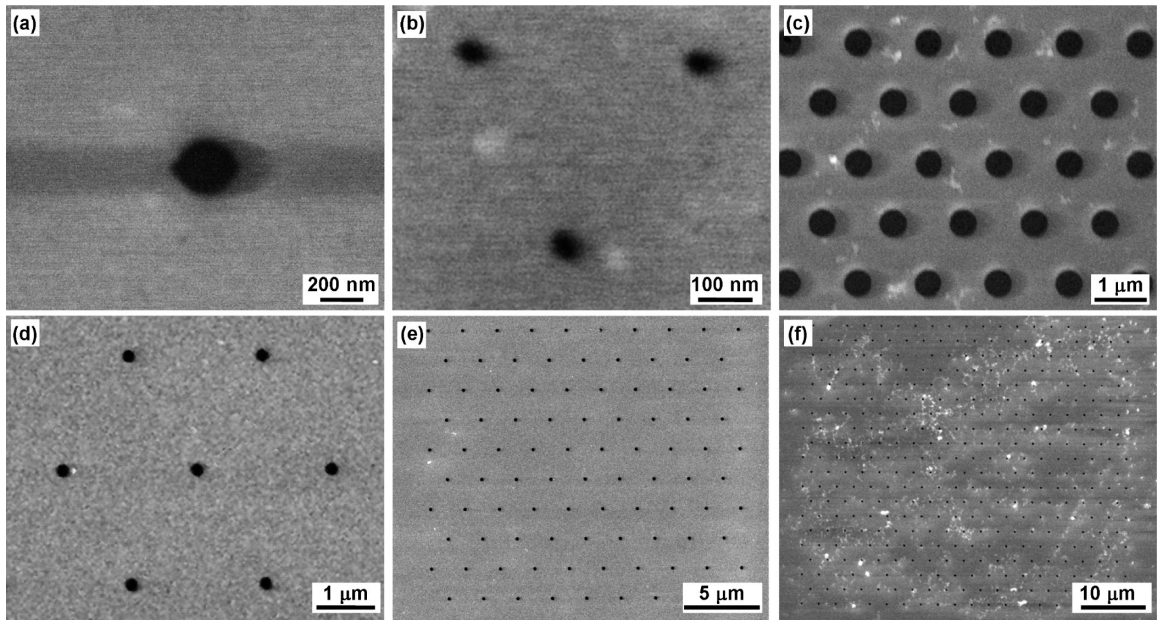

Figure 2. SEM images of a selection of nanopore arrays with different pore radius (r_a) and pore center-to-center separation (r_c), as listed in Table 1. (a) Single nanopore ($r_a \approx 125$ nm, design 2 from Table 1). (b) High magnification image of pores from the array with the smallest pore radius ($r_a \approx 25$ nm, $r_c \approx 495$ nm (20 r_a), design 8). (c) Part of an array (design 7) with $r_a \approx 225$ nm, $r_c \approx 1240$ nm (5 r_a). (d) Part of an array of pores fabricated using design 10 with $r_a \approx 125$ nm, $r_c \approx 2445$ nm (20 r_a). (e) Entire pore array (95 pores) for design 10. (f) Entire pore array (390 pores) for design 12 with $r_a \approx 115$ nm, $r_c \approx 2475$ nm (20 r_a).

silicon, patterning (by electron beam lithography) and etching of nanoscale pores in the Si_3N_4, selective thinning of the bulk silicon from underneath the Si_3N_4, and dicing the wafers into individual chips for experimentation. The Si_3N_4 membranes provided by this process were 100 nm thick, supported by a silicon frame which was 525 μm thick. The thin membrane was itself 500 μm × 500 μm, and the chip dimensions were 5 mm × 5 mm.

Figure 2 shows SEM images of typical membranes portraying the pore geometry and pore-to-pore relationships. The geometric parameters of each nanopore array studied electrochemically are listed in Table 1. Good pattern fidelity is evident, and in most cases (Figure 2a–e), only a small density of surface defects can be observed, likely due to processing residue. For arrays with the smallest pores ($r_a = 25$ nm, Figure 2b), precise determination of the pore shape was challenging, due to charging effects from the insulating substrate.

The hydrophobicity of the thinned Si_3N_4 membranes was assessed by measurement of its contact angle with deionized water. This was found to be 97 ± 3°, indicating that the surface of the silicon nitride membrane was hydrophobic. As we were unable to measure the contact angle inside the nanopores, an assumption must be made that the nanopore walls were also similarly hydrophobic, although this is not necessarily the case. The high surface-to-volume ratio may make the nanopores difficult to permeate with water and, thus, apparently more hydrophobic in practice than the membrane surface itself.[35]

The nanopore arrays were designed to yield a range of membranes, each with a unique value for the nanopore radius (r_a), the interpore (center–center) separation (r_c), and the total numbers of pores in the array (N_p). Values for r_a were chosen in the range 25 nm ≤ r_a ≤ 250 nm. For arrays with multiple pores, the interpore separation (r_c) was chosen to be a multiple of the pore radius, either $r_c = 5\ r_a$ or $r_c = 20\ r_a$, and the pores were arranged in a hexagonal pattern.

Table 1. Geometric Parameters of the Nanopore Array Membranes[a]

design	pore radius, r_a/nm	pore center-to-center separation		number of pores in the array, N_p
		r_c/nm	as a multiple of r_a	
1				0
2	120 ± 5			1
3	25 ± 5	125 ± 5	$5r_a$	95
4	45 ± 5	250 ± 5	$5r_a$	95
5	75 ± 5	375 ± 5	$5r_a$	95
6	120 ± 5	630 ± 10	$5r_a$	95
7	225 ± 5	1240 ± 25	$5r_a$	95
8	25 ± 5	495 ± 5	$20r_a$	95
9	65 ± 5	1455 ± 10	$20r_a$	95
10	125 ± 5	2445 ± 20	$20r_a$	95
11	230 ± 5	4905 ± 20	$20r_a$	95
12	115 ± 5	2475 ± 15	$20r_a$	390
13	65 ± 5			1
14	45 ± 5	915 ± 15	$20r_a$	23
15	50 ± 5	1040 ± 10	$20r_a$	95
16	55 ± 5	1090 ± 5	$20r_a$	390

[a] Data were obtained from SEM measurements. Pore radius (r_a) and pore center-to-center separation (r_c) are values averaged over six pores (with the exception of designs 1, 2, and 13). Resolution of the SEM measurements was ±5 nm.

Electrochemical Ion Transfer across the NanoITIES Arrays. Ion transfer across arrays of nanoscopic liquid–liquid interfaces localized within 100 nm thick Si_3N_4 membranes was characterized using cyclic voltammetry (CV). The transfer of TEA^+ across the ITIES is known to be reversible on the time scale of voltammetric experiments at millimeter-sized in-

(35) Bratko, D.; Daub, C. D.; Leung, K.; Luzar, A. *J. Am. Chem. Soc.* **2007**, *129*, 2504–2510.

terfaces[36,37] and at microinterfaces.[38] This transfer was chosen as the model reaction for the present studies. A variety of parameters inherent to the experimental setup influence the general shape of the observed CVs. These include (i) the geometric properties of the pores, such as r_a, r_c, N_p, and the thickness of the membrane (pore depth), l; (ii) the properties of the transferring ion species and the electrolyte solutions employed, such as the diffusion coefficient of TEA^+ in the aqueous and organic phases, D_{aq} and D_{org}, respectively, and the bulk concentration of TEA^+, C_j^*, in the aqueous phase; (iii) the location of the liquid−liquid interface within the pore, which depends mainly on the hydrophobicity and wetting properties of the nanoporous membrane material; and (iv) the electrical double layer present at the nanopore walls due to surplus charge at the surface (e.g., due to ion adsorption or charged surface groups). The surface potential due to this electrical double layer decays exponentially into the diffuse layer with a characteristic distance known as the Debye length (λ_D).[39] For a 10 mM LiCl aqueous electrolyte at 25 °C, the Debye length is ca. 10 nm. Using the relative dielectric constant of 1,6-DCH of 8.6,[40] the Debye length for the organic phase electrolyte of 10 mM (BTPPA)(TPBCl) in 1,6-DCH at 25 °C is ca. 1 nm. Considering the fact that the region of varying potential extends to a distance of about $3\lambda_D$ before the potential has decayed to about 2% of its value at the surface,[39] even at the smallest diameter of the pores (50 nm) studied here, the electrical double layer on the pore walls will have a minimal effect.

CVs were measured using scan rates v between 5 and 100 mV s^{-1}, both in the presence and absence (which defines the background current) of 150 μM TEA^+. Examples for $v = 5$ and $v = 50$ mV s^{-1} are given in Figure 3A,B for the nanoITIES array based on membrane design 12 (Table 1). Steady-state voltammograms were observed at all scan rates investigated for the forward scan (transfer of TEA^+ from the aqueous to the organic phase). After subtraction of the background current, the limiting currents were independent of the scan rate, indicating the dominance of spherical diffusion to the pores. Steady-state behavior was also observed for the back transfer of the TEA^+ ions from the organic phase to the aqueous phase; however, at higher scan rates, a peak-shaped voltammogram evolved. This behavior is evident from Figure 3C, which shows background-subtracted voltammograms for the reverse scan at scan rates between 5 and 100 mV s^{-1}. The appearance of current peaks during the reverse scan, where TEA^+ is transferred from the organic to the aqueous phase, indicates that the nanopores are filled with the organic phase and that the nanointerfaces are close to the pore orifices on the aqueous side or coplanar with the membrane on the aqueous side. In this situation, a portion of the TEA^+ transferred into the organic phase during the forward scan remains within the nanopore. Only a linear diffusion field can develop within the nanopores, which is manifested as a peak current. This situation is supported by the fact that the diffusion coefficient of the TEA^+ ion in the gelified organic phase is ca. 9 times lower than in the aqueous phase.[27] However, because of the short pore length, at longer time scales (slower scan rates), the TEA^+ ions will transport right through the nanopores and diffuse into the bulk organic phase. The time scale for an ion to traverse the nanopore is ca. 90 μs (using $l \approx (Dt)^{1/2}$, where l is the diffusion distance (pore length, 100 nm), D is the diffusion coefficient (1.13×10^{-6} cm^2 s^{-1} for TEA^+)[27] in the organic phase, and t is time), which is a lot shorter than the time available, ca. 100 s, at a 5 mV s^{-1} sweep rate. In such circumstances, the back transfer is dominated by spherical diffusion. This situation was previously investigated by simulations of ITIES confined within micropore arrays.[27,31] However, because we have a nanoITIES

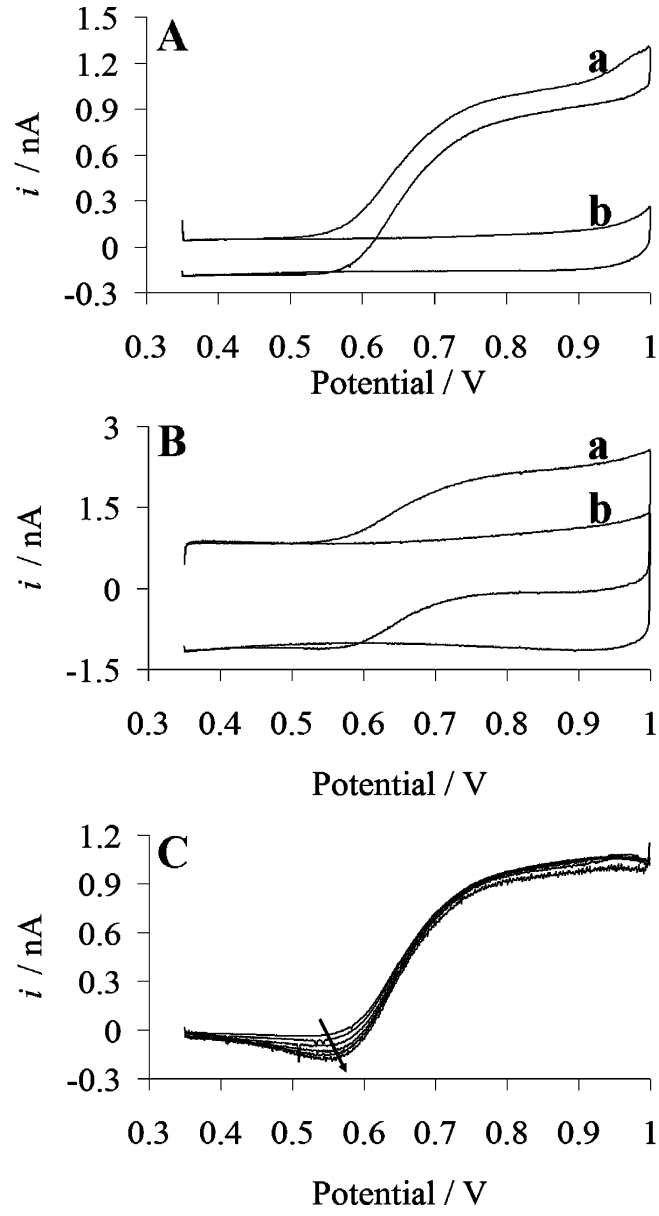

Figure 3. Cyclic voltammetry (CV) of 150 μM TEA^+ transfer as a function of scan rate at nanoITIES arrays formed using nanopore array design 12. CV responses are shown at scan rates of (A) 5 mV s^{-1} and (B) 50 mV s^{-1} for (a) 150 μM TEA^+ transfer and (b) blank. (C) Background subtracted CV responses for increasing scan rates (as indicated by the direction of the arrow) of 5, 10, 20, 35, 50, and 100 mV s^{-1} for the back transfer of 150 μM TEA^+.

(36) Samec, Z. *J. Electroanal. Chem.* **1979**, *99*, 197–205.
(37) Strutwolf, J.; Manzanares, J. A.; Williams, D. E. *Electrochem. Commun.* **1999**, *1*, 139–144.
(38) Rodgers, P. J.; Amemiya, S. *Anal. Chem.* **2007**, *79*, 9276–9285.
(39) Schoch, R. B.; Han, J.; Renaud, P. *Rev. Mod. Phys.* **2008**, *80*, 839–883.
(40) Katano, H.; Senda, M. *Anal. Sci.* **2001**, *17*, 1027–1029.

array here, diffusion zone overlap in the gelled organic phase is also present (as discussed below for the forward sweep).

If theories employed in the study of microelectrode arrays are applied to the nanoITIES arrays, the observation of steady-state behavior for the forward scan suggests that there is no overlap of diffusion zones formed at the pore orifices. These overlapped diffusion zones would suppress radial diffusion to the pores so that diffusion becomes gradually linear, resulting in a decreased current and the appearance of a peak-shaped voltammogram. Although the often used criterion $r_c > 20r_a$ for the absence of diffusion zone interaction[41] in microelectrode arrays is fulfilled in the array design used in Figure 3, this criterion is not applicable for values of $r_a < 1$ μm.[42] Recently, it was shown by computer simulation that steady-state voltammograms are achieved at nanoelectrode arrays[43] when radial diffusion to electrodes at the edges of the array dominates. These simulated steady-state voltammograms were achieved despite the presence of overlapped diffusion zones at nanoelectrodes within the array, away from the edges. The simulations were in agreement with experimental data from the same group[43] as well as from others.[44−49] As will be shown below, there is also substantial diffusion zone overlap at the nanoITIES arrays studied here, despite the absence of a current peak.

Closer examination of the as-recorded CVs of TEA^+ transfer across the nanoITIES array revealed that they did not display a true limiting current plateau on the forward sweep (Figure 3A,B). Instead, the current in the diffusion-limited region was seen to rise steadily with applied potential up to the switching potential, $\Delta_o^w\varphi_{sw}$. This phenomenon has been noted previously in CVs of ion transfer across μITIES[50,51] and may be attributable to movement of the aqueous-organogel nanointerfaces under potential stimulation. By imaging the interface with confocal laser scanning microscopy during CV measurements, Dale and Unwin demonstrated recently that the polarized liquid−liquid microinterface moves during charge transfer.[52] They noted that on the forward sweep the liquid−liquid interface had a slight oblate hemispheroidal shape, but in the diffusion-limited region approaching $\Delta_o^w\varphi_{sw}$, the interface gradually expanded outward and, thus, caused an increase in the current. The movement of the microinterface was completely reversible, contracting on the reverse sweep and adopting its initial configuration at the start of the next sweep. Such movement of the nanoITIES may be occurring in the results presented here, despite the gelification of the organic electrolyte phase such that it is more viscous than a liquid organic electrolyte phase. Additionally, the lack of a true limiting current plateau may be due to some elements of background electrolyte transfer at the higher potentials (e.g., ca. 0.95 V in Figure 3a) and to artifacts introduced by the background subtraction procedure employed.

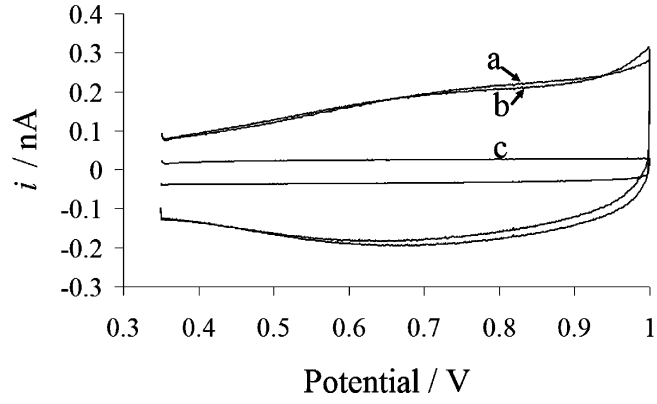

Figure 4. Comparison of the CV responses for a blank system (a) at nanoITIES array design 14, which contains 23 pores with pore radius (r_a) of 45 ± 5 nm; (b) at nanoITIES array design 1, which contains no pores; and (c) after replacing the nanoporous membrane chip in the experimental setup with an unpatterned (i.e., by e-beam lithography, photolithography, or wet-etching) 5 × 5 mm diameter chip of uniform ~525 μm thickness. This chip consisted of a 525 μm thick Si layer, 35 nm pad−oxide layer, and 100 nm Si_3N_4 layer. Scan rate used was 5 mV s^{-1}.

Some analysis of the resistance and capacitance of the nanoITIES membrane system may be beneficial in developing an understanding of its properties. Resistivity between the electrodes residing in each phase will lead to a potential drop (*iR* drop), and as a result, the potential applied by the potentiostat will deviate from the actual potential across the interface. Despite the application of automatic positive feedback compensation during the CV scans via the potentiostat, so as to minimize the effect of the resistance, Ohmic distortion of the background-subtracted CV is still evident in the rising part of the voltammogram, where the slope is lower than expected for a reversible ion-transfer process. However, this behavior can also be explained by a kinetically limited ion transfer, and the effects of both on the rising part of the current−voltage curve are difficult to separate.[53] Although TEA^+ is reported to undergo reversible transfer at micro-ITIES,[27,38] the higher mass-transfer coefficient at nanometer-scale interfaces might impart some kinetic limitations to ion transfer across the interface.[54−56]

To investigate the capacitance of the nanopore array system, the CV responses of a blank electrolyte solution system (i.e., in the absence of TEA^+) obtained at a membrane without pores (design 1) and at a nanoITIES array containing 23 pores, with $r_a \sim 45$ nm (design 14), are compared in Figure 4. The blank CVs in both cases are virtually identical. This implies that the nanopores have little influence on the overall capacitance.

A control experiment was also carried out to ensure that no leakage of electrolyte was taking place from one phase to the other, i.e., to ensure that the only water−organogel interfaces

(41) Saito, Y. *Rev. Polarogr.* **1968**, *15*, 177–187.
(42) Davies, T. J.; Compton, R. G. *J. Electroanal. Chem.* **2005**, *585*, 63–82.
(43) Godino, N.; Borriseé, X.; Munõz, F. X.; del Campo, F. J.; Compton, R. G. *J. Phys. Chem. C* **2009**, *113*, 11119–11125.
(44) Baker, W. S.; Crooks, R. M. *J. Phys. Chem. B* **1998**, *102*, 10041–10046.
(45) Ito, T.; Audi, A. A.; Dible, G. P. *Anal. Chem.* **2006**, *78*, 7048–7053.
(46) Sandison, M. E.; Cooper, J. M. *Lab Chip* **2006**, *6*, 1020–1025.
(47) Lanyon, Y. H.; Arrigan, D. W. M. *Sens. Actuators, B* **2007**, *121*, 341–347.
(48) Lanyon, Y. H.; De Marzi, G.; Watson, Y. E.; Quinn, A. J.; Gleeson, J. P.; Redmond, G.; Arrigan, D. W. M. *Anal. Chem.* **2007**, *79*, 3048–3055.
(49) Neluni, D. M.; Perera, T.; Ito, T. *Analyst* **2010**, *135*, 172–176.
(50) Stewart, A. A.; Taylor, G.; Girault, H. H.; McAleer, J. *J. Electroanal. Chem.* **1990**, *296*, 491–515.
(51) Shao, Y.; Mirkin, M. V. *Anal. Chem.* **1998**, *70*, 3155–3161.
(52) Dale, S. E. C.; Unwin, P. R. *Electrochem. Commun.* **2008**, *10*, 723–726.
(53) Bard, A. J.; Faulkner, L. R. *Electrochemical Methods: Fundamentals and Applications*, 2nd ed.; John Wiley and Sons Inc.: New York, 2001.
(54) Li, Q.; Xie, S.; Liang, Z.; Meng, X.; Liu, S.; Girault, H. H.; Shao, Y. *Angew. Chem., Int. Ed.* **2009**, *48*, 8010–8013.
(55) Rodgers, P. J.; Amemiya, S.; Wang, Y.; Mirkin, M. V. *Anal. Chem.* **2010**, *82*, 84–90.
(56) Wang, Y.; Velmurugan, J.; Mirkin, M. V.; Rodgers, P. J.; Kim, J.; Amemiya, S. *Anal. Chem.* **2010**, *82*, 77–83.

present were those to be found within the confines of the nanopore arrays. The nanoporous membrane chip in the experimental setup was replaced with an unpatterned 5 × 5 mm diameter chip of uniform ~525 μm thickness. This chip consisted of a 525 μm thick Si layer, 35 nm pad−oxide layer, and 100 nm Si_3N_4 layer. The CV responses for an unpatterned "blank" membrane (design 1) are compared with those attained for the unpatterned ~525 μm chip in Figure 4. The only difference between the experiments is that nanopore array design 1 contains the 100 nm thick Si_3N_4 membrane, whereas the unpatterned 5 × 5 mm chip is uniformly ~525 μm thick over its entire area. By assuming that in both cases, for the thin and the thick unpatterned Si_3N_4 membrane, the system can be described as a parallel plate capacitor, where the distance between the parallel plates is given by the thickness of the unpatterned membrane, a 5000 times higher capacitance current is expected for the 100 nm separation of the conducting phases compared to a 525 μm distance. This is not the case, as can be seen in Figure 4. The capacitance current shown for the thinner membrane is lower than expected if both membranes possessed the same electronic insulating properties. It may well be that the Si_3N_4 membrane is not an effective insulator between the organic and aqueous phases and on a subnanometer scale may be porous (e.g., via grain boundaries). This conclusion is supported by the fact that some features of ion transfer can be seen in the pore-free thin membrane (discussed later).

It can be concluded that the dominance of the capacitance in the CV measurements may be a limiting factor in analytical applications of these nanopore membranes, since the background current influences the detection limits. In this case, it appears that the three phase aqueous-silicon nitride-organogel structure controls the overall capacitance, which contributes to the background current, whereas the analytical signal, the diffusion-controlled faradaic current, is controlled by the pore geometry defined by e-beam lithography.

Influence of Nanopore Array Geometry. The electrochemical behavior of the nanoITIES arrays was examined in terms of the number of pores in the array (N_p), the pore radius (r_a), and the pore center-to-center separation (r_c). The greater steady-state current density, J_{ss}, generated at a miniaturized (micro- or nano-) ITIES is gained at the expense of a smaller analytical signal in the form of the absolute steady-state current, i_{ss}. This is due to the significant reduction in the area of the interface, A. Generally, the preferred strategy when dealing with this conundrum is to create arrays of interfaces by use, in the present case, of arrays of nanopores (i.e., to increase N_p). Ideally, the nanopores of these arrays will have noninteracting diffusion zones on the time scale of the voltammetric experiment. The absolute current is then simply the sum of the steady-state currents[41] of the individual pores in the array, if the liquid−liquid interface is inlaid[1,34,57]

$$i_{ss} = 4z_j F D_j C_j^* r_a N_p \quad (1)$$

where z_j, C_j^*, and D_j are the charge, bulk concentration, and diffusion coefficient, respectively, of the transferring ion in the aqueous phase and F is the Faraday constant (96 487 C mol^{-1}).

(57) Zoski, C. G. *Electroanalysis* **2002**, *14*, 1041–1051.

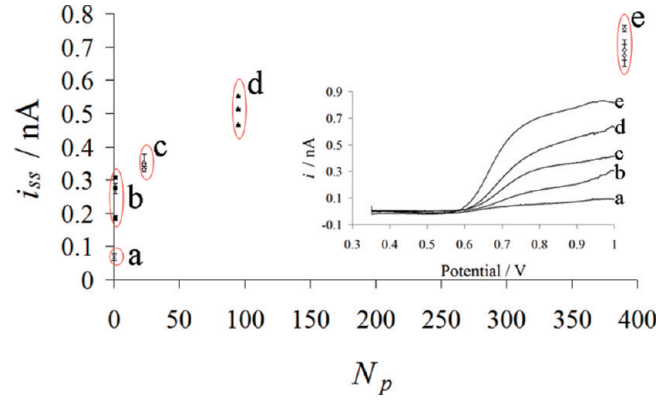

Figure 5. Variation of i_{ss} with N_p measured from the background subtracted steady-state CVs on the forward sweep for ion transfer of 150 μM TEA^+ across nanoITIES arrays formed using nanopore array designs 1 (a), 13 (b), 14 (c), 15 (d), and 16 (e). Three separate membranes were characterized for each nanopore array design to highlight the reproducibility of the CV response. Inset: Comparison of background subtracted CVs (forward sweep depicted only) of 150 μM TEA^+ transfer at nanoITIES arrays formed using the aforementioned nanopore array designs. Scan rate used was 5 mV s^{-1}.

A study of the effect of increasing N_p was undertaken, while maintaining a constant r_a of ca. 50 nm and r_c of 20r_a, with N_p values of 0, 1, 23, 95, and 390 pores (designs 1, 13, 14, 15, and 16; Table 1). The CV responses for the ion transfer of 150 μM TEA^+ and a blank electrolyte system were obtained, at a scan rate of 5 mV s^{-1}, for three individual chips at each nanopore array design and background-subtraction carried out (not shown). Steady-state behavior on the forward and reverse sweeps was observed for all nanopore array designs studied at this sweep rate. The expectation here was that, as N_p increased, i_{ss} would increase (eq 1) and that the resistance across the membrane would decrease. The pores of the array act like resistors in parallel. The total inverse resistance is estimated by multiplying the inverse resistance of a single pore by N_p, and thus, the resistance of the array, R_a, decreases with increasing N_p.

Nanopore array design 1, with no pores patterned in the 100 nm thick Si_3N_4 membrane, was investigated to see if TEA^+ ions could permeate the membrane and cause a resultant steady-state current to be observed. This experiment is based on the proposition that the current behavior observed at nanopore array design 1 in the absence of a transferring ion, Figure 4, may be due to a subnanometer porosity of the membrane not visible from the SEM images of each nanopore array design. As is evident from the background-subtracted forward sweep for nanopore array design 1 (inset, Figure 5a), some TEA^+ ions seem to be capable of diffusing across the membrane with a steady-state current of 0.067 (±0.010) nA. In contrast to the other nanopore array designs with e-beam fabricated pores, however, the steady-state current at nanopore array design 1 showed poor reproducibility.

The background-subtracted forward sweep voltammograms of each nanopore array design (with N_p values of 0, 1, 23, 95, and 390) are compared in the inset to Figure 5. Each nanopore array design was investigated using three different nanopore array membranes, and good reproducibility of the electrochemical signal between fabricated membranes was evident. A shift of $E_{1/2}$ to less

positive potentials occurred with increasing N_p as the array resistance decreased. i_{ss} increased with N_p but not in a linear fashion, as illustrated in Figure 5, suggesting diffusion zone overlap at r_c values of $20r_a$. This observation is not in agreement with the often-applied conditions for noninteracting diffusion zones at the micrometer-scale, $r_c > 12r_a$[41] and $r_c > 20\ r_a$,[58] but is in agreement with the results of Godino et al.,[43] who found that the average current per nanoelectrode (in their case) decreased with increasing electrode numbers in the array. In this case, the nanointerface array behaves essentially as a microinterface, with an effective radius equivalent to that of the total nano-ITIES array. In such circumstances, the trend in current with N_p shown in Figure 5 is similar to the trend in current with microinterface size, as calculated from eq 1. This indicates that the nanoITIES array is effectively behaving as a single micro-ITIES in the conditions employed here and that radial diffusion to nanoITIES at the edge of the array is dominant over linear diffusion to nanoITIES within the array.

At sufficiently long times, the diffusion layer thickness at a single nanoITIES is much larger than r_a, and the current is nonuniform over the interface. The local current density at the interface increases with decreasing distance from the edge (the "edge effect").[59] At steady state, the theoretical local current density at an infinitesimally small distance to the electrode edge indeed becomes infinite. Since the circular area of the ITIES scales with r_a^2, while the circumference scales with r_a, a decrease of the circular area leads to an increase of the current density. Thus, in order to investigate the effects of r_a and r_c on ion transfer at nanoITIES arrays, CV of the transfer of 150 μM TEA^+ and of blank electrolyte systems were undertaken using membrane designs with an identical N_p value of 95 but increasing r_a values in the range of 25 nm $\leq r_a \leq$ 250 nm. These increasing pore radius experiments were performed using two sets of membranes with pore center−center separations, r_c, of either $5r_a$ or $20r_a$.

The CV responses using a scan rate of 5 mV s^{-1} produced sigmoidal waves on both the forward and reverse sweep at all r_a and r_c values investigated. As outlined, for both of these data sets, two trends are expected: an increase in the absolute steady-state current (i_{ss}) and a decrease in the steady-state current density (J_{ss}) with increasing r_a. Both of these trends were observed, as shown in Figure 6.

The enhancement in J_{ss} obtained with a decrease in pore size (interface size) is the result of the beneficial enhanced mass transport, due to dominance of the edge effect. This enhanced J_{ss} at small interfaces is expected to be of benefit in bioanalytical detection methods as long as the effects of resistance, capacitance, and low absolute current can be addressed. The latter, of course, is achieved through use of arrays of interfaces. This in turn is influenced by the possibility of diffusion zone interaction at adjacent pores. From the data presented (Figure 6), it can be seen that an important feature of these experiments is that J_{ss} and i_{ss} are greater for the data set with the larger pore center-to-center separation, r_c, of $20r_a$. This is indicative of less diffusion zone overlap between adjacent pores at the arrays with greater pore center-to-center separations.

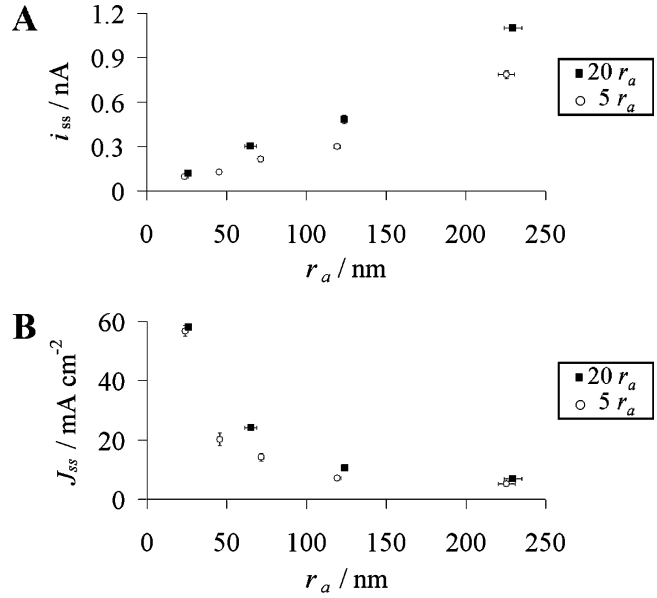

Figure 6. Effect of increasing pore radii (r_a) on the electrochemical ion-transfer response at pore center-to-center separations (r_c) of 5 or 20 times r_a. (A) Experimental steady-state currents, i_{ss}, measured from the background subtracted steady-state CVs on the forward sweep, and (B) the corresponding steady-state current densities, J_{ss} (mA cm^{-2}), for ion transfer of 150 μM TEA^+ through pores of the indicated pore radius (r_a) with r_c values as a multiple of either 5 times r_a (hollow circles, ○: nanoITIES array designs 3, 4, 5, 6, and 7) or 20 times r_a (solid squares, ■: nanoITIES array designs 8, 9, 10, and 11). Scan rate used was 5 mV s^{-1}.

The extension of the diffusion zone around an individual nanoITIES under potential scanning conditions and, hence, the degree of diffusion zone overlap for an array of nanoITIES, can only be estimated by inclusively considering the influences of the pore radius (r_a), the applied scan rate (v), and the diffusion coefficients of the transferring species in both phases (D_{aq} and D_{org}).[27] Whether this is a reasonable approach depends on whether the ion transfer at the nanoITIES is described by diffusion-only mass transport theory. White and co-workers have reported that voltammetric behavior of nanometer-sized electrodes with $r_a > 10$ nm is consistent with mass transport by Fickian diffusion.[60,61] However, for $r_a < 10$ nm, deviations of the electrochemical response from that predicted by theories based only on diffusional transport occur.[60,61] Therefore, diffusion equations suffice for description of mass transport at the nanoITIES arrays studied here, all of which have pores with radius $\geq$ 25 nm.

Attempts have been made to quantify the degree of diffusion zone overlap at gellified μITIES arrays[27] and at microelectrode arrays,[41,42,62] but as yet no universal model exists that allows accurate estimation of diffusion zone overlap when $r_a < 1\ \mu$m. As mentioned above, Godino et al.[43] found by simulation and experiment that diffusion to the edge of a nanoelectrode array was more important, leading to steady-state voltammograms even when diffusion zone overlap occurred, although they were unable to study large numbers of pores by simulation. This is the situation with the nanoITIES

(58) Fletcher, S.; Horne, M. D. *Electrochem. Commun.* **1999**, *1*, 502–512.
(59) Oldham, K. B. *J. Electroanal. Chem.* **1981**, *122*, 1–17.
(60) Conyers, J. L.; White, H. S. *Anal. Chem.* **2000**, *72*, 4441–4446.
(61) White, R. J.; White, H. S. *Langmuir* **2008**, *24*, 2850–2855.
(62) Menshykau, D.; Huang, X.-J.; Rees, N. V.; Campo, F. J. d.; Munoz, F. X.; Compton, R. G. *Analyst* **2009**, *134*, 343–348.

arrays reported here also. For the present study, a qualitative approach toward describing the diffusion zone overlap at nanoITIES arrays is applied here. As discussed above, J_{ss} and i_{ss} are greater for the data set with an r_c spacing of $20r_a$ (Figure 6). When the diffusion layer thickness $\delta > 0.5r_c$, the diffusion zones around adjacent nanoITIES overlap. Within these overlapping areas, the individual nanoITIES compete with each other for incoming analyte species, effectively depleting the same area, referred to as the depletion or exclusion zone. The presence of these exclusion zones leads to a drop in J_{ss} and i_{ss} for an array compared to the situation where $\delta < 0.5r_c$. As the nanoITIES move progressively closer together, to a situation where $\delta \gg 0.5r_c$, complete overlap of diffusion zones will occur and a linear concentration profile will be established. The data in Figure 6 indicate a greater degree of overlap of diffusion zones, with the corresponding drop in J_{ss} and i_{ss}, as we move from an r_c value of $20r_a$ to $5r_a$. Nevertheless, current peaks were not observed in either data set for the forward sweep, as would be expected at the micrometer-scale if linear diffusion to the ITIES was occurring, again highlighting the fact that radial diffusion to the edge of a nanointerface array is dominant over linear diffusion to nanoITIES within the array. Regardless, we know from the influence of N_p on the ion-transfer current that overlap does occur at an r_c value of $20r_a$, and logically, this overlap is greater at an r_c of $5r_a$.

The nanoelectrode array simulations presented by Godino et al.[43] agree very well with the experimental data presented here for ion-transfer voltammetry. They reported that (i) diffusion zone overlap occurred for the case of $r_c = 60\ r_a$, which is greater than the value of r_c employed here, 20 r_a; (ii) as r_c decreased, greater diffusion zone overlap occurred, as shown by a decreased steady-state current; (iii) as the number of nanoelectrodes in the array increased, the average current per nanoelectrode decreased; and (iv) the sigmoidal voltammograms at the nanoelectrode arrays exhibited a near-independence from scan rate in the experimentally accessible range available at the nanoITIES arrays (i.e., $\nu \leq 200\ mVs^{-1}$). All of these results are in agreement with the experimental data for nanoITIES arrays presented here.

CONCLUSIONS

This work combined nanofabrication and electrochemistry in the development of new membranes of potential use in biosensing and chemical sensing. The first geometrically regular arrays of nanoscale liquid−liquid interfaces have been developed and characterized. Nanoporous Si_3N_4 membranes fabricated by a combination of photolithographic patterning, wet-etching, e-beam lithographic patterning, and gas phase reactive ion etching were used to define the nanoITIES array. The voltammetric behavior of the nanoITIES arrays in the presence of a transferring ion was characterized by CV. Apparent steady-state behavior was observed on the forward and reverse sweeps at all nanoITIES array geometries irrespective of the pore center-to-center separations. From the data presented, it is evident that diffusion zone overlap between adjacent nanopores does in fact occur on the transfer of TEA^+ from the aqueous to organic even for arrays with the larger pore center-to-center separations. However, the peak-shaped response on the forward CV sweep, expected if microscale theories of diffusion zone overlap are applied, was not observed. This behavior can be rationalized on the basis that an array of nanoITIES exhibiting diffusional zone overlap seems to behave as a single microscale ITIES with an area of similar dimensions to that occupied by the nanoITIES array, as suggested for nanoelectrode arrays.[43] This is due to the dominance of radial diffusion which occurs to pores at the edges of the array, which seems to be more important than linear diffusion to pores within the array. Steady-state voltammetry was observed here for nanoITIES arrays containing up to 390 nanointerfaces. NanoITIES arrays with the smaller pore center−center separation, at 5 times the radius, exhibited lower steady-state currents, consistent with greater diffusion zone overlap. Background-subtracted CVs confirmed the evolution of a peak-shaped response on the reverse CV sweep with increasing scan rate, where TEA^+ is transferred from the organogel back to the aqueous phase, indicating that the pores are filled with the organogel. The capacitance of the nanoporous membrane may be a limiting factor in analytical applications of such ion-transfer electrochemistry at nanoITIES since it contributes to the background current and will influence the detection limits achievable. The 100 nm thick Si_3N_4 membrane may contain subnanoscale pores, not seen under SEM imaging, leading to a small ionic conductivity over the entire 500 μm × 500 μm thin membrane. For analytical applications of voltammetry, the analytical signal, based on the diffusion-controlled faradaic current, is controlled by the e-beam defined pore area, but the background signal, which has an impact on achievable detection limits, is dominated by the capacitance. Despite this possible drawback, the current density was seen to increase with decreasing nanointerface size, which should result in enhanced sensitivity for analytical detection. This aspect will be explored in further studies. The results presented here show how electron-beam lithography and associated methods may be combined with ion-transfer electrochemistry as a basis for voltammetric detection. Possible future applications of these devices include the electrochemical detection of nonredox active ions.

ACKNOWLEDGMENT

This work was supported by Science Foundation Ireland (Grant Number 07/IN.1/B967), the Irish Research Council for Science, Engineering, and Technology (Embark Postgraduate Research Scholarship Scheme, Grant Number RS/2005/122), and the European Commission (Marie Curie Transfer of Knowledge Programme, Grant Number MTKD-CT-2005-029568). Fabrication facilities were supported by the Programme for Research in Third Level Institutions. The staff of the Central Fabrication Facility at Tyndall National Institute are thanked for the preparation of the membranes employed in this work, especially Mr. Joe O'Brien for his meticulous attention to detail during proTEKB3 application and removal. Technical support received from Brewer Science Inc. (Montana) regarding the use of proTEKB3 is gratefully acknowledged.

SUPPORTING INFORMATION AVAILABLE

Schematic diagram of the electrochemical cell setup. This material is available free of charge via the Internet at http://pubs.acs.org.

Received for review March 30, 2010. Accepted May 31, 2010.

AC1008282